PERGAMON

International Journal of Heat and Mass Transfer 43 (2000) 3775–3784

International Journal of HEAT and MASS TRANSFER

www.elsevier.com/locate/ijhmt

Thermoconvective instability in a bounded vertical cylinder with internal heat generation

K.F. Wu*, J.P. Brancher

Laboratoire d'Energétique et de Méchanique Théorique et Appliquée, CNRS, URA 875, 2, Avenue de la Forêt de Haye, B.P. 160, 54504 Vandoeuvre Cedex, France

Received 2 June 1997; received in revised form 4 January 2000

Abstract

The onset of thermal convection of a fluid confined completely in a finite vertical cylinder with internal heat source is examined by using the linear stability analysis. The Galerkin method is applied to solve the perturbation equations. The stability criteria for various aspect ratios are determined in terms of the Rayleigh number and a nondimensional parameter relative to the heat source. The effects of the aspect ratio and the sidewall thermal boundary conditions on the stability as well as the structure of the convective roll are investigated. In the limiting cases, the results compare well with the literature.

1. Introduction

The onset of thermal convection in a closed circular cylinder is now well documented for fluids without internal heat generation [1–5]. On the contrary, the stability of a fluid with internal heat source has only received attention in the case of horizontal fluid layer [6–11], plane vertical fluid layer [12,13], inclined fluid layer [14,15] and infinite long coaxial cylinder [16,17]. For the geometry of a finite vertical cylinder, the investigations are still restricted to porous medium [18] in which the velocity field is simplified so as to obey the Darcy equation. A good summary of convection in cylindrical geometry without internal heat source and in fluid layer heated internally can be found in [19].

This work was motivated by the examination of the thermal convection in a cylindrical sole electrode which contains a conductive fluid (steel) submitted to Joule heating by a current. Neither theoretical nor experimental study has been found in the open literature concerning the convective instability of a fluid in a closed vertical cylinder with internal heat source. Previous attention has been paid by Wu et al. [20] with the aide of a numerical simulation by imposing a physically possible gravity perturbation. This is the only set of results to which our present linear analysis with internal heat source can be compared. The numerical simulation with internal heat source presented in [20] has been validated in a horizontal fluid layer and the results agree with that of the linear analysis of [6]. Although the experiment investigations are not available, the direct simulation can still be regarded as a kind of numerical experiment. However, their results are limited to axisymmetric convection. The goal of this work was, therefore, to provide a complete linear stability analysis including the possibility of non-axisymmetric flows at the onset of thermal convection in a closed vertical cylinder with internal heat source.

When a horizontal fluid layer is heated from below, it is well known that the temperature distribution of the equilibrium state is linear and the threshold of the

* Corresponding author.

0017-9310/00/$ - see front matter
PII: S0017-9310(00)00019-3

instability can be determined by means of a single nondimensional parameter: the Rayleigh number *Ra*.

$$Ra = \frac{g\beta l^3 \delta T}{\nu\alpha} \tag{1}$$

where g is the gravitation acceleration, ν the kinematic viscosity, α the thermal diffusivity, β the coefficient of thermal expansion, l the characteristic length-generally equal to the depth of the layer H and δT is the characteristic temperature difference. Usually, in the heating-from-below problem, $\delta T = T_L - T_H > 0$ is the difference of the lower surface temperature T_L and the upper surface temperature T_H. With the presence of internal heat source, the temperature distribution of the quiescent state is nonlinear and this basic state can break down whether the upper surface temperature is inferior or superior to the lower one provided that a sufficiently large negative temperature gradient appears somewhere within the fluid in spite of the simultaneous existence of the positive temperature gradient. Another nondimensional parameter which was defined originally by Sparrow et al. [6] in the case of the horizontal fluid layer can represent the heat source effect:

$$Sp = \frac{SH^2}{2k\delta T} \tag{2}$$

where k is the thermal conductivity and S the uniformly distributed internal heat generation (energy/volume-time). $\delta T = T_L - T_H$ may be positive, negative or equal to zero. *Sp* has not had a name so far to the authors' knowledge. In homage to his pioneer contribution in the field of hydrodynamic instability with internal heat source, from now on, we will call it Sparrow number. A parameter $(g\beta SH^5)/(2k\nu\alpha)$ called internal Rayleigh number Ra_I by some researchers is the product of Sparrow number and Rayleigh number.

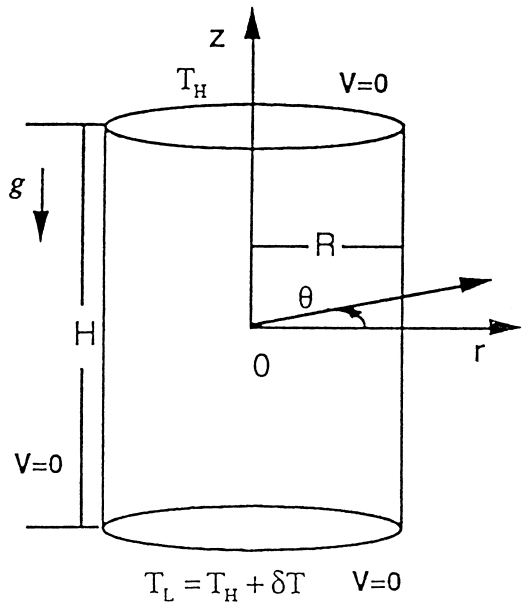

Fig. 1. Diagram of physical system.

2. Mathematical formulation

The system to be studied consists of an initially motionless Boussinesq fluid which fills a rigid vertical circular cylinder of height H, radius R with uniform internal heat source S as shown in Fig. 1. The perfectly conducting lower and upper surfaces are maintained at constant temperatures T_L and $T_H = T_L - \delta T$, respectively. The lateral boundary is assumed to be adiabatic or the conducting sidewall is kept at the temperature of the equilibrium state of the fluid.

The initial velocity, temperature, pressure and density are those under steady state conditions:

$$V_0 = 0 \tag{3}$$

$$T_0 = \frac{S}{2k}\left(\frac{H^2}{4} - z^2\right) + \left(\frac{T_H + T_L}{2} - \frac{\delta T}{H} z\right) \tag{4}$$

$$\nabla P_0 = -\rho_m g\left[1 - \beta\left(\lambda z + \frac{S}{2k}\left(z^2 + \frac{H^2}{12}\right)\right)\right]\boldsymbol{e}_z \tag{5}$$

$$\rho_0 = \rho_m\left[1 - \beta\left(\lambda z + \frac{S}{2k}\left(z^2 + \frac{H^2}{12}\right)\right)\right] \tag{6}$$

where $\lambda = -Sz/k - \delta T/H$ is the initial temperature gradient, ρ_m the initial mean density, and $\boldsymbol{e}_z$ the unit vector along the z axis. The nonlinear temperature distribution in the fluid depends only on z. The quiescent state temperature distribution is linear when $S = 0$ corresponding to the problem of a fluid heated from below.

If the marginal state is assumed to be time independent, the linearized nondimensional perturbation equations in which V, P and T are the disturbances of the velocity, pressure and temperature are:

$$\nabla \cdot \boldsymbol{V} = 0 \tag{7}$$

$$\nabla^2 \boldsymbol{V} + Ra T \boldsymbol{e}_z - \nabla P = 0 \qquad Ra = g\beta H^3 \delta T/\nu\alpha \tag{8}$$

$$\nabla^2 T + \boldsymbol{V} \cdot \boldsymbol{e}_z(2Sp\bar{z} + 1) = 0 \qquad Sp = SH^2/2k\delta T \tag{9}$$

where ∇^2 is the Laplace operator, *Ra* the Rayleigh number and *Sp* the Sparrow number. The perturbed velocity $\boldsymbol{V}$, temperature T and pressure P are measured

in units of α/H, δT and $\rho_0\alpha\nu/H^2$, respectively. Thermal diffusivity α and kinematic viscosity ν were assumed constants in the above derivation. The radial and vertical coordinates $\bar{r}$ and $\bar{z}$ are scaled by R and H. This scaling introduces the aspect ratio $A = R/H$ into the differential operators. The boundary conditions are:

$$\boldsymbol{V} = 0 \quad \text{on all surfaces} \tag{10}$$

$$T = 0 \quad \text{on} \quad \bar{z} = \pm 1/2 \tag{11}$$

$$\frac{\partial T}{\partial \bar{r}} = 0 \quad \text{on} \quad \bar{r} = 1 \quad \text{(insulating sidewalls)} \tag{12}$$

or

$$T = 0 \quad \text{on} \quad \bar{r} = 1 \quad \text{(conducting sidewalls)} \tag{13}$$

3. Solution of stability equations

Eqs. (7)–(9) and the boundary conditions (10)–(13) constitute an eigenvalue problem for the Rayleigh number Ra. For a given value of Sparrow number Sp and aspect ratio A, there is a maximum eigenvalue corresponding to the critical Rayleigh number Ra_c, marking the onset of instability.

3.1. Symmetric mode

The Galerkin's method is used to generate an approximate solution. For each variable, the approximating series are expressed as:

$$T = \sum_i \sum_l B_{il} T_{il} \tag{14}$$

$$V = \sum_i \sum_l E_{il} \boldsymbol{V}_{il} \tag{15}$$

where B_{il} and E_{il} are constants. T_{il} and V_{il} are the temperature and velocity trial functions which satisfy the boundary conditions. The temperature trial function is chosen as follows:

$$T_{il} = \left(\bar{z}^2 - 1/4\right)\bar{z}^{l-1} J_0\left(\beta_i \bar{r}\right) \tag{16}$$

where J_0 is the Bessel function of the first kind of order zero, β_i the ith root of $J_1(\beta_i) = 0$ for the insulating sidewalls or the ith root of $J_0(\beta_i) = 0$ for the conducting sidewalls. The velocity trial function is derived from a stream function ψ_{il}:

$$\boldsymbol{V_{il}} = \nabla \times \left(\psi_{il} \boldsymbol{e}_\theta\right) \tag{17}$$

The boundary conditions on the stream functions ψ_{il} are:

$$\psi_{il} = \frac{\partial \psi_{il}}{\partial \bar{r}} = 0 \quad \text{on} \quad \bar{r} = 1 \tag{18}$$

$$\psi_{il} = \frac{\partial \psi_{il}}{\partial \bar{z}} = 0 \quad \text{on} \quad \bar{z} = \pm 1/2 \tag{19}$$

$$\psi_{il} = 0 \quad \text{at} \quad \bar{r} = 0 \tag{20}$$

Eq. (20) is obtained on demanding the solution to be finite everywhere. The stream functions ψ_{il} are therefore chosen as:

$$\psi_{il} = \left(\bar{z}^2 - 1/4\right)^2 \bar{z}^{l-1} \left(\frac{J_1(\eta_i \bar{r})}{J_1(\eta_i)} - \frac{I_1(\eta_i \bar{r})}{I_1(\eta_i)} \right) \tag{21}$$

J_1, I_1 are the Bessel function and modified Bessel function of the first kind of order one. η_i is the ith root of

$$J_1(\eta_i) I_2(\eta_i) + I_1(\eta_i) J_2(\eta_i) = 0 \tag{22}$$

in order to satisfy the condition of a rigid lateral wall. Note that pressure will vanish from the Galerkin formulation due to the solenoidal form of the velocity fields. Therefore, its representation is not specified.The Galerkin technique requires the residual to be orthogonal to each appropriate trial function. We substitute Eqs. (14) and (15) into Eqs. (8) and (9). Then we multiply the resulting momentum equation by $\boldsymbol{V}_{jm}$, and energy equation by T_{jm} and perform the volume integration. This procedure yields a set of algebraic equations. In matrix form:

$$\begin{bmatrix} & \boldsymbol{M}_{11} & \boldsymbol{M}_{12} \\ Ra & \boldsymbol{M}_{21} & \boldsymbol{M}_{22} \end{bmatrix} \begin{bmatrix} \boldsymbol{B} \\ \boldsymbol{E} \end{bmatrix} = 0 \tag{23}$$

The definitions of the matrices are:

$$\begin{aligned} M_{11} &= \int_\Omega T_{jm} \nabla^2 T_{il} \, \mathrm{d}\Omega \\ \boldsymbol{M}_{12} &= \int_\Omega T_{jm} \boldsymbol{V}_{il} \cdot \boldsymbol{e}_z (2Sp\bar{z} + 1) \, \mathrm{d}\Omega \\ \boldsymbol{M}_{21} &= \int_\Omega \boldsymbol{V_{jm}} \cdot \boldsymbol{e}_z T_{il} \, \mathrm{d}\Omega \\ \boldsymbol{M}_{22} &= \int_\Omega \boldsymbol{V_{jm}} \cdot \nabla^2 \boldsymbol{V_{il}} \, \mathrm{d}\Omega \end{aligned} \tag{24}$$

where Ω is the axisymmetric domain: $-1/2 \le \bar{z} \le 1/2$, $0 \le \bar{r} \le 1$. Without heat source, $\boldsymbol{M}_{12}$ is the transpose of $\boldsymbol{M}_{21}$. The corresponding eigenvalue formulation is obtained by eliminating $\boldsymbol{B}$

$$\left(\boldsymbol{M}_{22}^{-1}\boldsymbol{M}_{21}\boldsymbol{M}_{11}^{-1}\boldsymbol{M}_{12} - I/Ra\right)\boldsymbol{E} = 0 \tag{25}$$

The largest eigenvalue is therefore the critical Rayleigh number Ra_c for a given Sparrow number and an aspect ratio. After the associated eigenvector $\boldsymbol{E}$ has been found, the vector $\boldsymbol{B}$ may be recovered from:

$$\boldsymbol{B} = -\boldsymbol{M}_{11}^{-1}\boldsymbol{M}_{12}\boldsymbol{E} \tag{26}$$

3.2. Asymmetric mode

The approximating series for temperature is:

$$T = \sum_i \sum_l D_{il} T_{il} \tag{27}$$

where D_{il} are expansion coefficients and the temperature trial function T_{il} is chosen as:

$$T_{il} = \cos(n\theta)\left(\bar{z}^2 - \frac{1}{4}\right)\bar{z}^{l-1} J_n\left(\beta_{ni}\bar{r}\right) \tag{28}$$

where n is the azimuthal mode number, J_n is the Bessel function of the first kind of order n, β_{ni} is the ith root of the following characteristic equations:

$$nJ_n\left(\beta_{ni}\right) - \beta_{ni}J_{n+1}\left(\beta_{ni}\right) = 0 \quad \text{(insulating sidewalls)} \tag{29}$$

$$J_n\left(\beta_{ni}\right) = 0 \quad \text{(conducting sidewalls)} \tag{30}$$

The velocity obtained by the superposition of two two-dimensional approximated velocity field is expressed by:

$$\boldsymbol{V} = \boldsymbol{V}^{(a)} + \boldsymbol{V}^{(b)} \tag{31}$$

where

$$\boldsymbol{V}^{(a)} = \sum_i \sum_l F_{il} \boldsymbol{V}_{il}^{(a)} \tag{32}$$

$$\boldsymbol{V}^{(b)} = \sum_i \sum_l G_{il} \boldsymbol{V}_{il}^{(b)} \tag{33}$$

F_{il} and G_{il} are constants; $\boldsymbol{V}_{il}^{(a)}$ and $\boldsymbol{V}_{il}^{(b)}$ are derived from stream functions ϕ_{il} and ψ_{il} so that continuity is automatically satisfied.

$$\boldsymbol{V}_{il}^{(a)} = \nabla \times \left(\phi_{il}\boldsymbol{e}_r\right) \tag{34}$$

$$\boldsymbol{V}_{il}^{(b)} = \nabla \times \left(\varphi_{il}\boldsymbol{e}_z\right) \tag{35}$$

The boundary condition on the stream functions are given by:

$$\varphi_{il} = \phi_{il} = \frac{\partial \varphi_{il}}{\partial \bar{r}} = 0 \quad \text{on} \quad \bar{r} = 1 \tag{36}$$

$$\varphi_{il} = \phi_{il} = \frac{\partial \phi_{il}}{\partial \bar{z}} = 0 \quad \text{on} \quad \bar{z} = \pm\frac{1}{2} \tag{37}$$

The finiteness of solutions everywhere requires:

$$\varphi_{il} = \phi_{il} = 0 \quad \text{at } \bar{r} = 0 \tag{38}$$

Trial functions that satisfy the above conditions are chosen as follows:

$$\phi_{il} = \sin(n\theta)\left(\bar{z}^2 - 1/4\right)^2 \bar{z}^{l-1} J_{n+1}(\sigma_i \bar{r}) \tag{39}$$

$$\begin{aligned}\varphi_{il} = {} & \sin(n\theta)\left[\left(\bar{z}^2 - 1/4\right)^2 - \left(\bar{z}^2 - 1/4\right)\right] \\ & \times \bar{z}^{l-1}\left(\frac{J_n(\xi_i\bar{r})}{J_n(\xi_i)} - \frac{I_n(\xi_i\bar{r})}{I_n(\xi_i)}\right)\end{aligned} \tag{40}$$

where I_n is the modified Bessel function of the first kind of order n. σ_i and ξ_i are respectively the roots of the following two characteristic equations:

$$J_{n+1}(\sigma_i) = 0 \tag{41}$$

$$J_n(\xi_i)I_{n+1}(\xi_i) + I_n(\xi_i)J_{n+1}(\xi_i) = 0 \tag{42}$$

The Galerkin method applied to Eqs. (8) and (9) generates a system of algebraic equation by requiring the residual to be orthogonal to each of the appropriate trial functions:

$$\begin{bmatrix} & \boldsymbol{M}_{11} & \boldsymbol{M}_{12} & 0 \\ Ra & \boldsymbol{M}_{21} & \boldsymbol{M}_{22} & \boldsymbol{M}_{23} \\ & 0 & \boldsymbol{M}_{32} & \boldsymbol{M}_{33} \end{bmatrix} \begin{bmatrix} \boldsymbol{D} \\ \boldsymbol{F} \\ \boldsymbol{G} \end{bmatrix} = 0 \tag{43}$$

where

$$\boldsymbol{M}_{11} = \int_\Omega T_{jm}\nabla^2 T_{il}\,\mathrm{d}\Omega$$

$$\boldsymbol{M}_{12} = \int_\Omega T_{jm}\boldsymbol{V}_{il}^{(a)} \cdot \boldsymbol{e}_z(2Sp\bar{z} + 1)\,\mathrm{d}\Omega$$

$$\boldsymbol{M}_{21} = \int_\Omega \boldsymbol{V}_{jm}^{(a)} \cdot \boldsymbol{e}_z T_{il}\,\mathrm{d}\Omega \qquad \boldsymbol{M}_{22} = \int_\Omega \boldsymbol{V}_{jm}^{(a)} \cdot \nabla^2 \boldsymbol{V}_{il}^{(a)}\,\mathrm{d}\Omega$$

$$\boldsymbol{M}_{23} = \int_\Omega \boldsymbol{V}_{jm}^{(a)} \cdot \nabla^2 \boldsymbol{V}_{il}^{(b)}\,\mathrm{d}\Omega \qquad \boldsymbol{M}_{32} = \int_\Omega \boldsymbol{V}_{jm}^{(b)} \cdot \nabla^2 \boldsymbol{V}_{il}^{(a)}\,\mathrm{d}\Omega$$

$$\boldsymbol{M}_{33} = \int_\Omega \boldsymbol{V}_{jm}^{(b)} \cdot \nabla^2 \boldsymbol{V}_{il}^{(b)}\,\mathrm{d}\Omega \tag{44}$$

and Ω is the asymmetric domain: $-1/2 \le \bar{z} \le 1/2$, $0 \le \bar{r} \le 1$, $0 \le \theta \le 2\pi$. Without heat source, the problem

is reduced to the conventional auto-adjoint problem of heating from below. Eliminating $\boldsymbol{D}$ and $\boldsymbol{G}$ yields the corresponding eigenvalue formulation:

$$\left[\left(\boldsymbol{M}_{22}-\boldsymbol{M}_{23}\boldsymbol{M}_{33}^{-1}\boldsymbol{M}_{32}\right)^{-1}\boldsymbol{M}_{21}\boldsymbol{M}_{11}^{-1}\boldsymbol{M}_{12}-I/Ra\right]\boldsymbol{F}=0 \tag{45}$$

For a given Sparrow number and an aspect ratio, the critical Rayleigh number is the largest eigenvalue. After the associated eigenvector $\boldsymbol{F}$ has been found, the vector $\boldsymbol{D}$ and $\boldsymbol{G}$ may be recovered from

$$\boldsymbol{D}=-\boldsymbol{M}_{11}^{-1}\boldsymbol{M}_{12}\boldsymbol{F} \tag{46}$$

$$\boldsymbol{G}=-\boldsymbol{M}_{33}^{-1}\boldsymbol{M}_{32}\boldsymbol{F} \tag{47}$$

4. Results and discussion

4.1. Comparison with the existing results in the limit cases of $Sp = 0$ and $Sp = \infty$

In order to validate the numerical procedure, the calculation was performed first in the case of symmetric mode for $Sp = 0$ and $Sp = \infty$ that correspond respectively to the classical problem of a fluid heated from below ($Sp = 0$) and the problem of the zero Rayleigh number convection ($|Sp| = \infty, \delta T = 0$). When $|Sp| = \infty$, i.e., $\delta T = 0$, the Rayleigh number is not a significant parameter of transition. We apply a modified Rayleigh number defined by

$$Ra_{\mathrm{m}} = g\beta(T_{\max}-T_{\mathrm{H}})(H/2-z_{\max})^3/(\nu\alpha) \tag{48}$$

or

$$Ra_{\mathrm{m}} \cong \frac{g\beta S H^5}{64k\nu\alpha} \quad \text{for } |Sp|\to\infty \quad (\delta T\to 0) \tag{49}$$

where $z_{\max}$ is the vertical coordinate of the maximum temperature $T_{\max}$. The critical modified Rayleigh number Ra_{mc} is obtained directly from the computed critical Rayleigh number Ra_{c} by a simple algebraic relation:

$$Ra_{\mathrm{mc}} = \frac{1}{32}\left(1+\frac{1}{Sp}\right)^3\left(Sp+\frac{1}{Sp}+2\right)Ra_{\mathrm{c}} \quad Sp\neq 0 \tag{50}$$

or

$$Ra_{\mathrm{mc}} \cong \frac{Sp}{32}Ra_{\mathrm{c}} = \frac{1}{32}Ra_{\mathrm{cI}} \quad \text{for } |Sp|\to\infty \quad (\delta T\to 0) \tag{51}$$

Table 1
Comparison of the critical Rayleigh numbers Ra_{c}, with values reported by Charlson and Sani [1] and Yamaguchi et al. [4]. All the results presented are based on the linear analysis of the stability

Sidewall	Aspect ratio A	This work: Galerkin method (no. of radial functions × no. of vertical functions)	Ref. [1]: Rayleigh–Ritz method (no. of radial functions × no. of vertical functions)	Ref. [4]: finite element method (finite element mesh)
Insulating wall	0.5	10873.15 (7 × 7)	10887.15 (10 × 3)	10892 (4 × 8)
	2.0	1862.17 (7 × 7)	1862.27 (10 × 3)	1871 (8 × 4)
	6.0	1725.91 (10 × 10)	1725.98 (10 × 3)	–
Conducting wall	0.5	11715.20 (7 × 7)	11725.08 (10 × 3)	–
	2.0	1886.13 (7 × 7)	1886.24 (10 × 3)	–
	6.0	11725.08 (10 × 10)	1726.25 (10 × 3)	–

Table 2
Comparison of the critical modified Rayleigh numbers Ra_{mc}, calculated by the linear analysis with values obtained by the numerical simulation

Aspect ratio A	Ref. [20]: numerical simulation	This work: linear analysis	
	$SP = \infty$ ($Pr = 0.1$)	$Sp = 1 \times 10^6$	$Sp = -1 \times 10^6$
0.5	1510.09	1545.70	1545.70
0.75	768.87	794.17	794.17
1.5	604.14	642.13	642.13
2.0	584.38	608.40	608.40

$SpRa_c = Ra_{cI}$ is the critical internal Rayleigh number. The comparison with the literature is presented in Tables 1 and 2.

The slightly higher values of Ra_c obtained by Yamaguchi et al. [4] presented in Table 1 may be due to the relatively coarse discretizations. Increasing the number of elements in the mesh can lead to more accurate results. The lower values of Ra_{mc} obtained by Wu et al. [20] presented in Table 2 may result from the low Prandtl number ($Pr = 0.1$) of the fluid under simulation.

For asymmetric mode without internal heat source, the Ra_c predicted is in agreement with that in [3,5,21] but does not agree with [2]. Buell and Catton [3] have explained that the azimuthal velocity is not well represented in [2]. The structure of the flow field at the onset of convection without internal heat source found in our linear analysis is in accordance with [1,4], for the axisymmetric mode and [5] for the asymmetric mode. With internal heat source, the axisymmetric mode compares well with [20].

The critical Rayleigh numbers are accurate to fourth significant figure for the symmetric mode by using the 49th order expansions (seven radial and seven vertical functions) based on the increment of total number of terms by 68. For the asymmetric mode, 72 terms were needed and nine radial with eight vertical terms gave the best results.

4.2. Critical Rayleigh numbers for $|Sp| = 100$

In order to illustrate the case with internal heat source of finite intensity, we chose the case $Sp = 100$ and $Sp = -100$ corresponding to the positive and negative temperature difference between the two horizontal surfaces confining the domain. The critical Rayleigh numbers for some selected aspect ratios with $|Sp| = 100$ are listed in Table 3. It is well known that for small aspect ratios, the critical mode is asymmetric in the heated-from-below case. Our results show that it remains true when there is an internal heat source with $|Sp| = 100$. The asymmetric mode $n = 1$ predominate when the aspect ratios A is inferior to about 0.75. For a large aspect ratio the difference of Ra_c between symmetric and asymmetric mode is reduced. The variation of Ra_c with aspect ratio A (between 1 and 4) for symmetric mode ($n = 0$) with $|Sp| = 100$ is presented in Fig. 2.

4.3. Velocity fields at the onset of convection

The system of perturbation equations and boundary conditions is invariant under the transformation $(Sp, \bar{z}) \rightarrow (-Sp, -\bar{z})$. The degree of this symmetry is strong when $|Sp|$ is large and the symmetry is exact for $|Sp| \rightarrow \infty$ regardless of the aspect ratio. When $Sp = 0$ the system is symmetric with respect to $\bar{z} = 0$ itself.

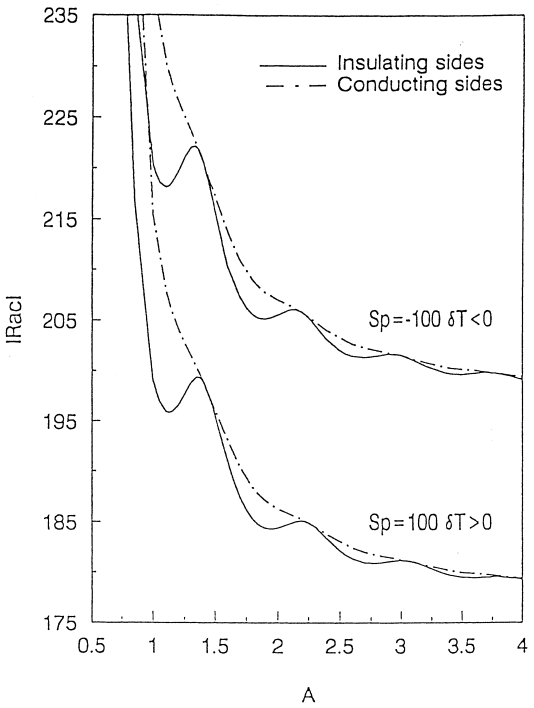

Fig. 2. The critical Rayleigh numbers for symmetric mode, $|Sp| = 100$, $1 \leq A \leq 4$.

Table 3
Critical Rayleigh number for some aspect ratios and for different modes, at $Sp = 0, 100, -100$

Sp	A	Mode *n*	Insulating sidewalls	Conducting sidewalls
0	4.0	0	1748.70	1749.53
		1	1733.95	
		2	1747.92	
		3	1741.66	
100	4.0	0	179.29	179.38
		1	178.75	
		2	179.17	
		3	178.96	
	1.5	0	195.68	196.28
		1	186.88	191.88
		2	193.86	196.58
		3	205.64	206.22
	0.5	0	480.77	531.01
		1	281.25	440.39
		2	441.97	
		3	771.16	
	0.25	0	3161.13	3384.86
		1	830.49	1879.82
		2	2480.52	4527.92
		3	5672.62	
−100	4.0	0	−199.21	−199.46
		1	−198.95	
		2	−199.05	
		3	−199.27	
	1.5	0	−215.78	−217.20
		1	−208.23	−213.08
		2	−213.46	−216.96
		3	−226.58	−226.56
	0.5	0	−509.11	−562.73
		1	−308.33	−473.45
		2	−471.17	
		3	−812.44	
	0.25	0	−3282.02	−3517.33
		1	−875.83	−1969.51
		2	−2583.08	−4702.50
		3	−5878.00	

The variations of the flow patterns depending not only on the aspect ratio but also on the Sparrow number is rather complex. We present here only some representative cases. The sidewalls are all adiabatic for all the flow fields presented below.

For a given aspect ratio $A \geq 1$, the number of axisymmetric rolls increases as *Sp* increases. An example of $A = 3.6$ is illustrated in Fig. 3 showing the characteristics of the increase of the wave number with increasing *Sp*. This is in agreement with the results of an infinite horizontal fluid layer [6] in which the wave length is 1.28 times larger for $Sp = 0$ than that for $Sp = \infty$.

For $|Sp| = 100$, a new circular roll occurs at the upper corner for $\delta T > 0$ or the lower corner for $\delta T < 0$ when the aspect ratio exceeds a value near the maxima of the insulating neutral curves in Fig. 2. The boundary of the new circular roll extends as the aspect ratio increases further. The roll having less velocity intensity can grow to a size roughly equal to its parallel counter-rotating roll when the aspect ratio nears a value corresponding to the minima of the neutral curves in Fig. 2. An example of the transition sequence from one to two rolls is shown in Fig. 4.

5. Conclusion

This study gives a linear stability analysis of a fluid in a bounded vertical cylinder with internal heat generation.

In each section, we have given partial conclusions

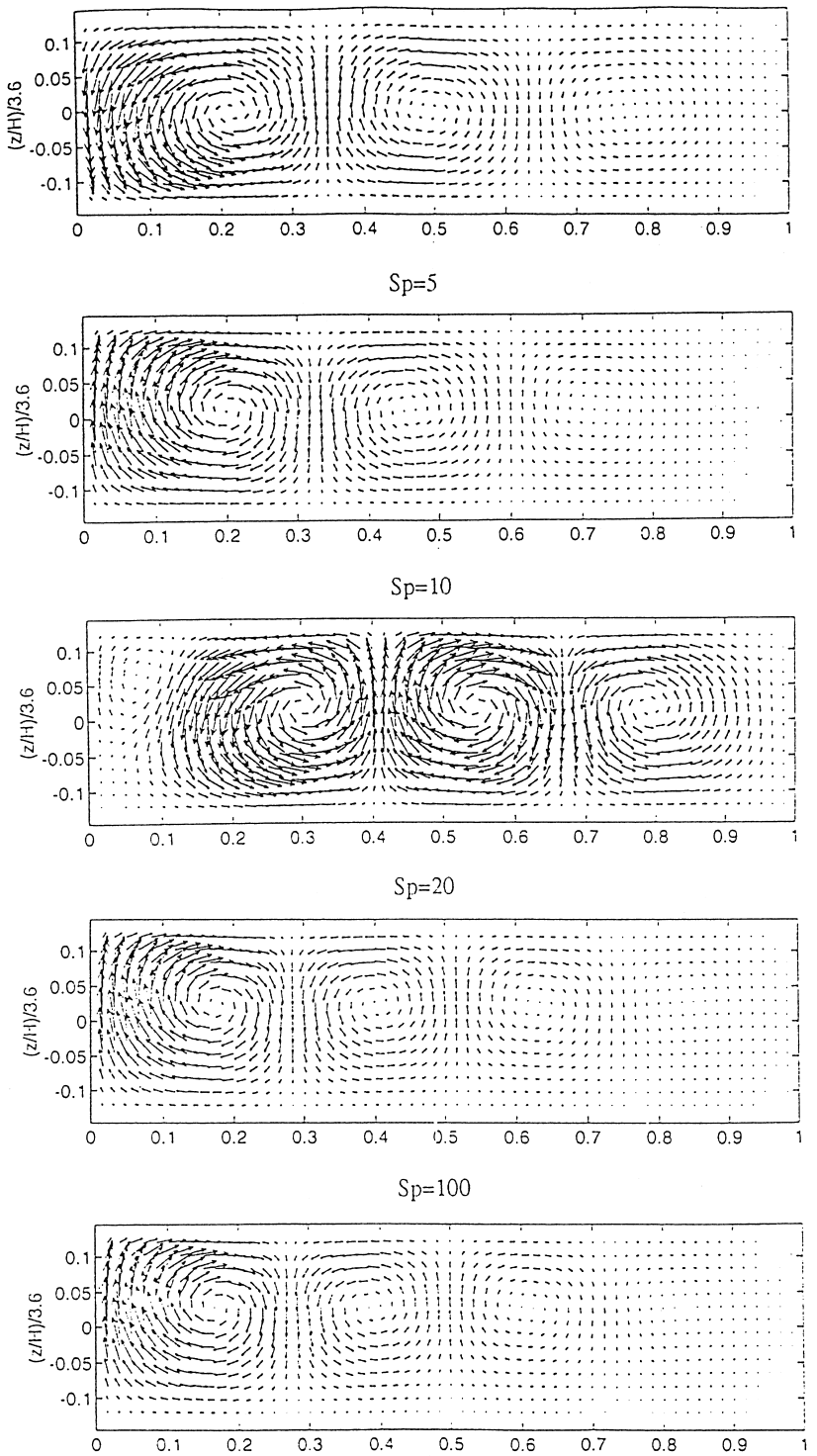

Fig. 3. The evolution of the velocity vectors as a function of *Sp* for a given aspect ratio $A = 3.6$, symmetric mode.

and results on the stability conditions for the symmetric and asymmetric modes depending on the aspect ratio and the internal heat generation.

In the limiting classical case without internal source, our results are compared with those in the literature, for all aspect ratios and different modes. For the symmetric mode with internal source, the comparison is done with a direct simulation we did in a previous paper. All these results are in good agreement.

The main points of the conclusion concerning the present study are that: the symmetry relative to the medium horizontal plane is broken, the Rayleigh number is not the only relevant parameter and, as in the classical case without source, the first asymmetric mode is the most unstable for small aspect ratios.

In the case without internal source, the heat can be transferred from the top to the bottom or vice versa depending on δT. In the case with internal heat source, the energy coming from the interior is transferred to the top and to the bottom. The conductive temperature distribution can have a region where the gradient is directed toward the bottom. So, the equilibrium becomes potentially unstable. If the top is hotter than the bottom and as the unstable domain is near the top, the effects of convection are to evacuate more energy toward the top (it is possible to obtain 70% of heat [20]). From the point of view of the dimensional analysis the two parameters that intervene when the two types of heat transfer are competitive, are the Rayleigh number Ra and the dimensionless number Sp which we call the Sparrow number.

The confinement has a stabilizing effect, but it is the asymmetric mode $n = 1$ that becomes more unstable than the axisymmetric mode for small aspect ratios. If the lateral wall is conductive, the stabilizing effect of the sidewall is weaker since the heat can be transferred laterally. On the contrary, in the adiabatic case, the heat cannot be evacuated toward the sidewalls. This creates a more favorable condition for the instability. In these two cases, the effect of the confinement is of little importance for the aspect ratio A superior to or of the order of 4.

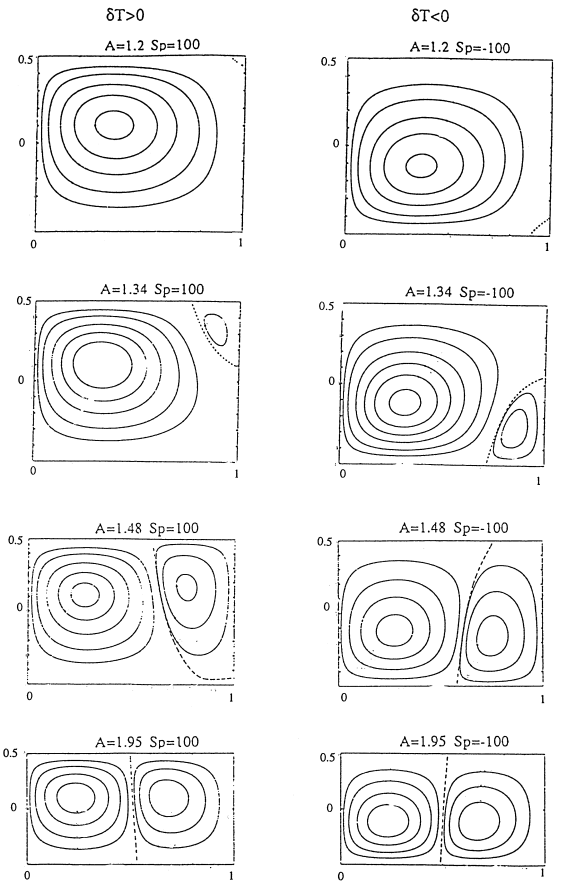

Fig. 4. Transition sequence from one to two rolls, insulating sidewall, $|Sp| = 100$.

References

[1] G.S. Charlson, R.L. Sani, Thermoconvective instability in a bounded cylindrical fluid layer, Int. J. Heat Mass Transfer 13 (1970) 1479–1496.

[2] G.S. Charlson, R.L. Sani, On thermoconvective instability in a bounded cylindrical fluid layer, Int. J. Heat Mass Transfer 14 (1971) 2157–2160.

[3] J.C. Buell, I. Catton, The effect of wall conduction on the stability of a fluid in a right circular cylinder heated from below, Trans. ASME J. Heat Transfer 105 (1983) 255–260.

[4] Y. Yamaguchi, C.J. Chang, R.A. Brown, Multiple buoyancy-driven flows in a vertical cylinder heated from below, Phil. Trans. R. Soc. Lond. 312 (1984) 519–552.

[5] G.R. Hardin, R.L. Sani, D. Henry, B. Roux, Buoyancy-driven instability in a vertical cylinder: binary fluids with Soret effect. Part 1: general theory and stationary stability results, International Journal for Numerical Methods in Fluids 10 (1990) 79–117.

[6] E.M. Sparrow, R.J. Goldstein, V.K. Jonsson, Thermal instability in a horizontal fluid layer: effect of boundary conditions and nonlinear temperature profile, J. Fluid Mech. 18 (1964) 513–528.

[7] P.H. Robert, Convection in horizontal layers with internal heat generation — theory, J. Fluid Mech. 30 (1967) 33–49.

[8] D.J. Tritton, M.N. Zarraga, Convection in horizontal layers with internal heat generation. Experiments, J. Fluid Mech. 30 (1967) 21–37.

[9] P.M. Waston, Classical cellular convection with a spatial heat source, J. Fluid Mech. 32 (1968) 399–411.

[10] F.A. Kulacki, R.J. Goldstein, Thermal convection in a horizontal fluid layer with uniform volumetric energy sources, J. Fluid Mech. 55 (1972) 271–287.

[11] N. Rudraiah, G.N. Sekhar, Convection in magnetic fluids with internal heat generation, Trans. ASME J. Heat Transfer 113 (1991) 122–127.
[12] G.Z. Gershuni, E.M. Zhukhovitskii, A.A. Iakimov, On the stability of steady convective motion generated by internal heat source, Sov. J. Appl. Math. Mech. 34 (1970) 669–674 (English translation).
[13] G.Z. Gershuni, E.M. Zhukhovitskii, A.A. Iakimov, Two kinds of instability of stationary convective motion induced by internal heat sources, Sov. J. Appl. Math. Mech. 37 (1973) 544–548 (English translation).
[14] M. Takashima, The stability of natural convection in an inclined fluid layer with internal heat generation, J. Phys., Soc. Jpn 58 (1989) 4431–4440.
[15] M. Takashima, The stability of natural convection in an inclined fluid layer with internal heat generation II, J. Phys., Soc. Jpn 60 (1991) 445–465.
[16] A.A. Kolyshkin, R. Vaillancourt, Stability of internally generated thermal convection in a tall vertical annulus, Can. J. Phys 69 (1991) 743–748.
[17] A.A. Kolyshkin, R. Vaillancourt, On the stability of nonisothermal circular Couette flow, Phys. Fluids 5 (1993) 3136–3146.
[18] W.E. Stewart Jr, C.L.G. Dona, Free convection in a heat-generating porous medium in a finite vertical cylinder, Trans. ASME J. Heat Transfer 110 (1988) 517–520.
[19] G.Z. Gershuni, E.M. Zhukhovitskii, Convective stability of incompressible fluids (translated from Russian), in: Israel Program for Specific Translation, Keter Publishing House, Jerusalem, 1976.
[20] K.F. Wu, E. Combeau, J.P. Brancher, Instabilité thermo-convective dans un cylindre avec source volumique de chaleur, Int J. Heat Mass Transfer 40 (1997) 1535–1543.
[21] M.N. Sarby, An integral method for studying the onset of natural convection, Eur. J. Mech., B/Fluids 12 (1993) 337–365.